Electronic Supplementary Information

Copper selenide/amino hyperbranched polymer as an organic/inorganic hybrid composite cathode for rechargeable magnesium batteries

Lin Ran[a], Hao Li[a], Fei Xu[c], Daohong Zhang[a,b]*, Ting Li[a,b]*

[a] Key Laboratory of Catalysis and Energy Materials Chemistry of Ministry of Education & Hubei Key Laboratory of Catalysis and Materials Science, Hubei R&D Center of Hyperbranched Polymers Synthesis and Applications, South-Central Minzu University, Wuhan 430074, China.

[b] Guangdong Provincial Laboratory of Chemistry and Fine Chemical Engineering Jieyang Center, Jieyang 515200, China

[c] Key Laboratory of Hydraulic Machinery Transients, Ministry of Education, School of Power and Mechanical Engineering, Wuhan University, Wuhan 430072, China.

* E-mail:

Ting Li (liting@mail.scuec.edu.cn)

Daohong Zhang (daohong.zhang@scuec.edu.cn)

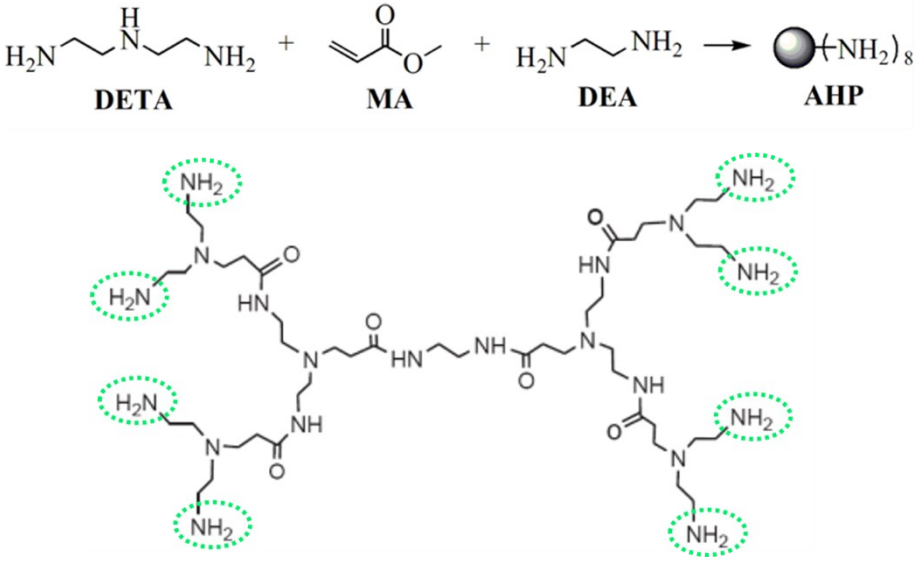

Fig. S1. Synthesis scheme and structure of AHP.

The synthesis process of amino hyperbranched polymer (AHP) is: a certain molar ratio of diethylenetriamine and methyl acrylate were added to methanol, and the mixture was stirred and reacted at 5 ℃ for 12 h. After dropwise addition of ethylenediamine, the mixture was reacted at 80 ℃ for 1 h and then at 130 ℃ for 8 h under nitrogen atmosphere to obtain liquid AHP.

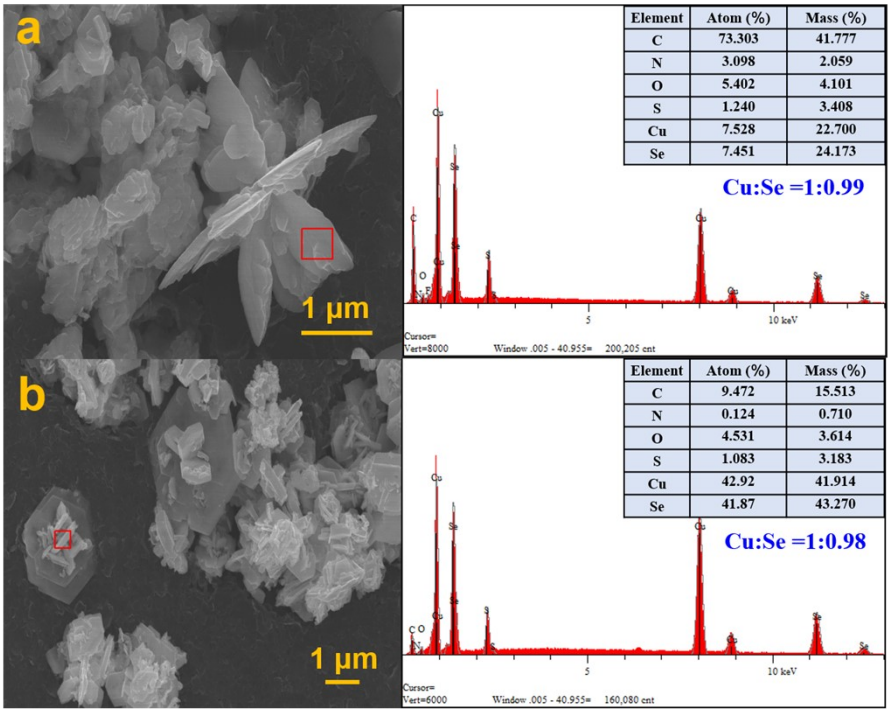

Fig. S2. EDS spectra of (a) CuSe-AHP and (b) CuSe samples.

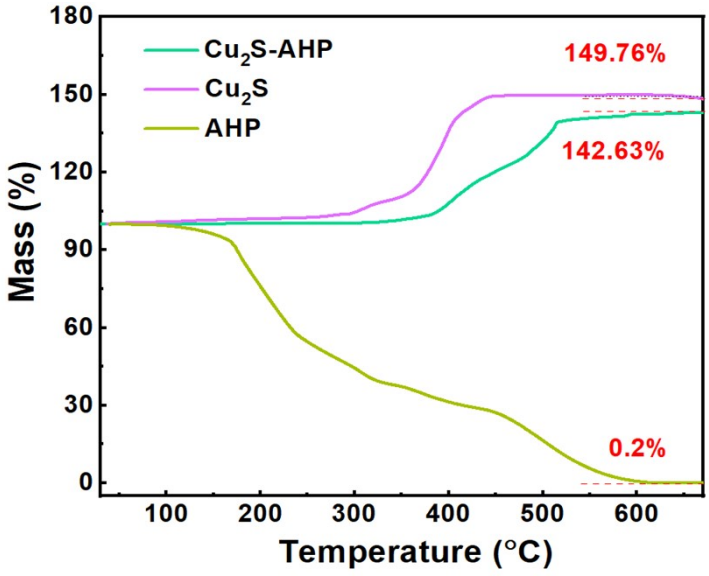

Fig. S3. TGA curves of AHP, Cu_2S and Cu_2S-AHP.

Pure Cu_2S gets weight increase of 49.76% at 650 ℃, which is consistent with the theoretical mass increase (oxidation to CuO and $CuSO_4$), while AHP loses weight (99.8%) due to the decomposition. As a result, the mass change of Cu_2S-AHP at 650 ℃ (42.63% increase) originates from the mass loss of AHP and mass increase of Cu_2S, and thus the content of AHP in Cu_2S-AHP is calculated to be 4.8 wt%.

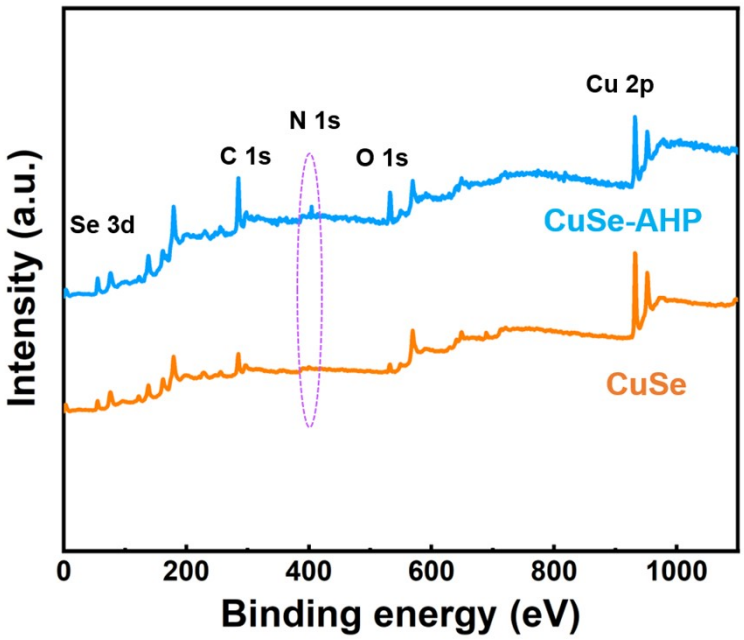

Fig. S4. Overall XPS spectra of CuSe-AHP and CuSe.

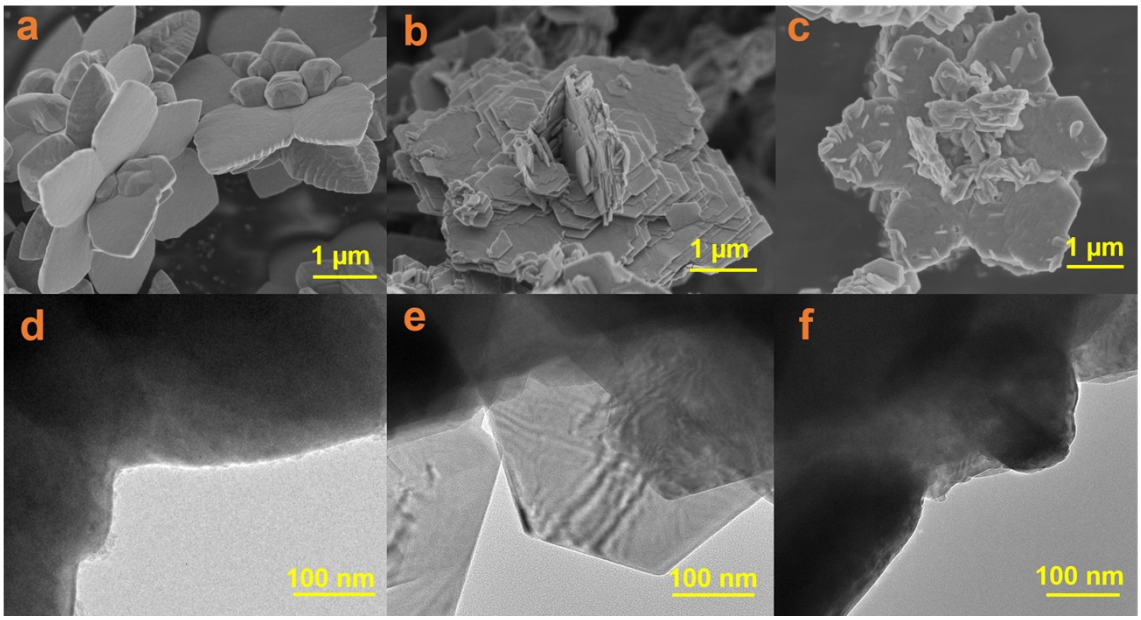

Fig. S5. SEM images of (a) Cu_2S-AHP, (b) CuSe-AHP and (c) CuSe. TEM images of (d) Cu_2S-AHP, (e) CuSe-AHP and (f) CuSe.

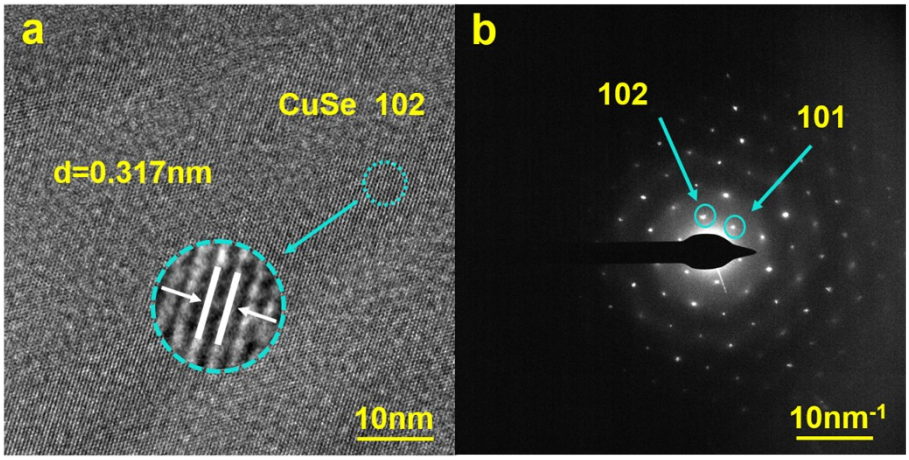

Fig. S6. (a) HRTEM image and (b) corresponding SAED pattern of CuSe.

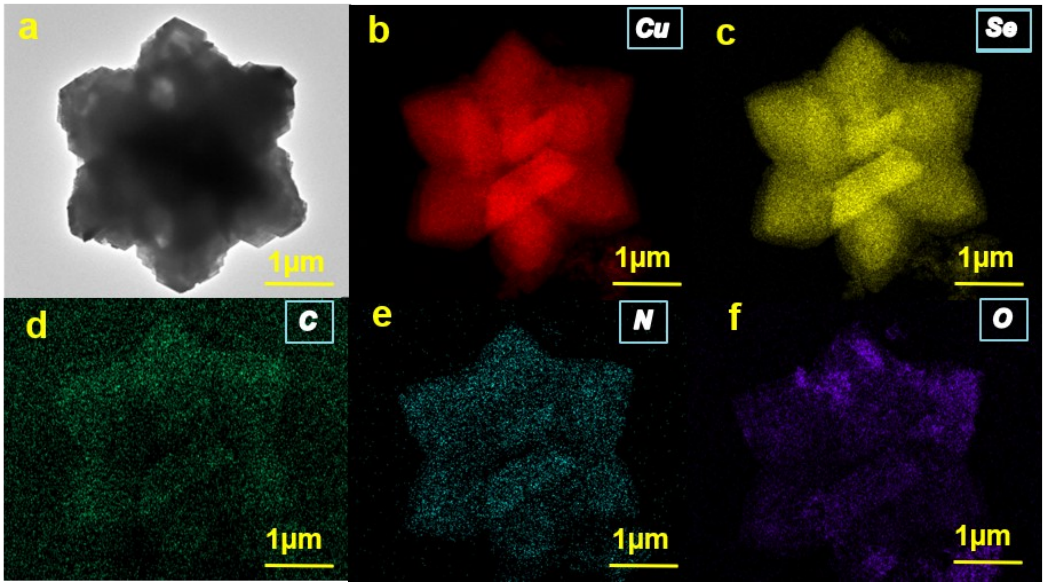

Fig. S7. (a) TEM image and (b-f) corresponding elemental (Cu, Se, C, N, O) mapping images of Cu_2S-AHP.

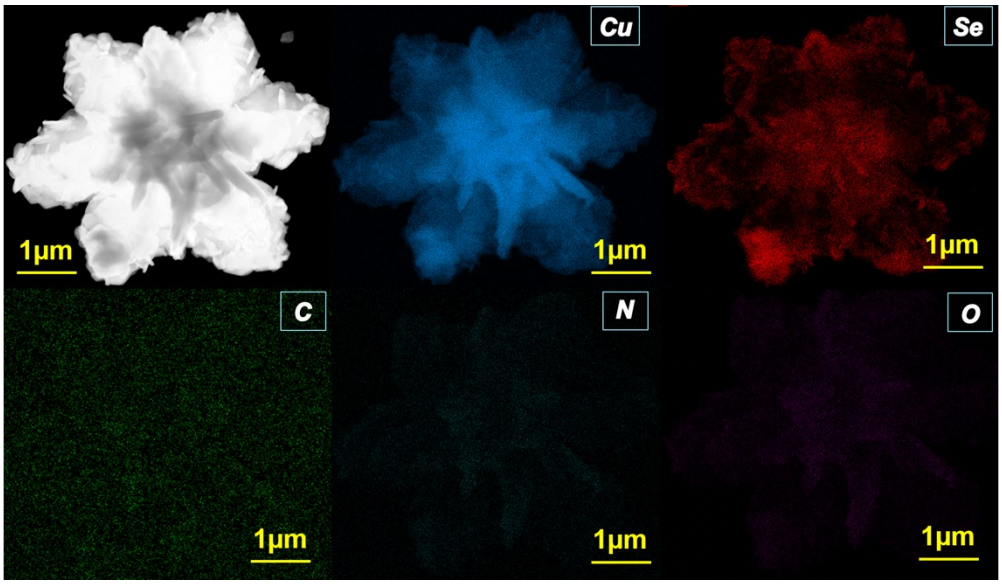

Fig. S8. HAADF STEM image and corresponding elemental (Cu, Se, C, N and O) mapping images of CuSe.

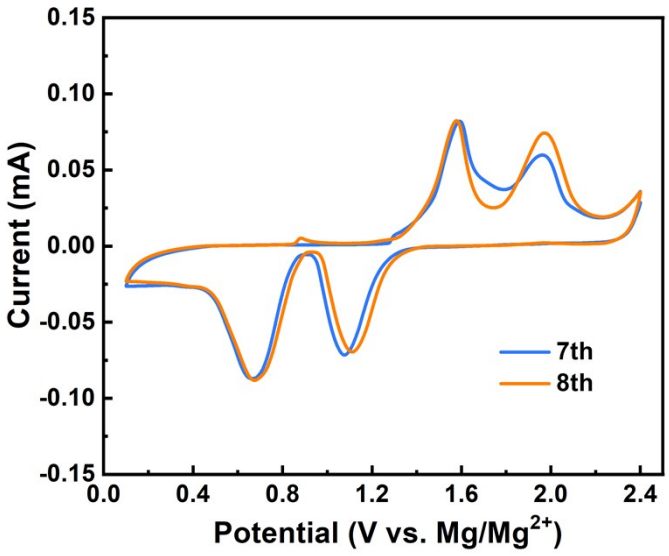

Fig. S9. CV curves of CuSe-AHP electrode at the 7th and 8th cycles (0.1 mV s^{-1})

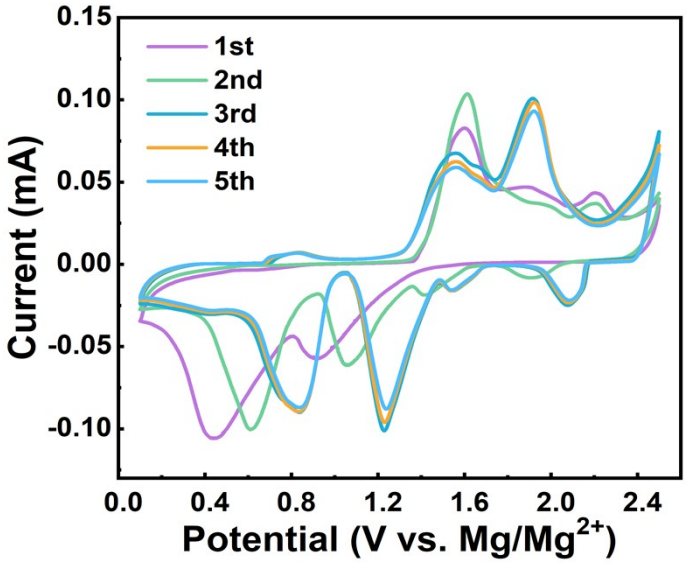

Fig. S10. CV curves of CuSe electrode at 0.1 mV s^{-1}.

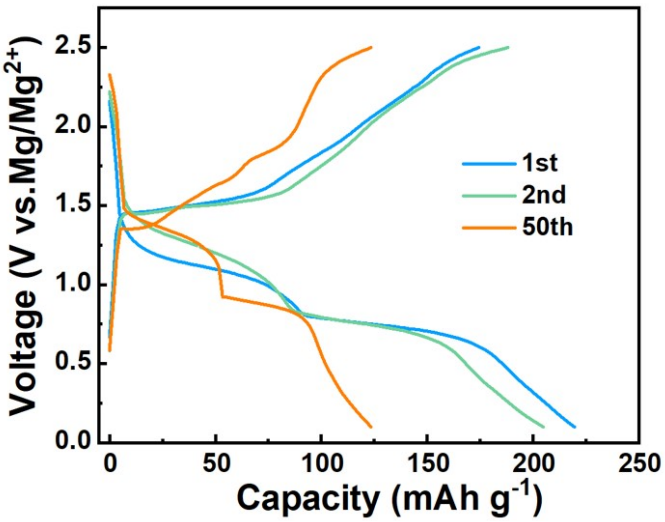

Fig. S11. Charge/discharge profiles of CuSe electrode at 100 mA g^{-1}.

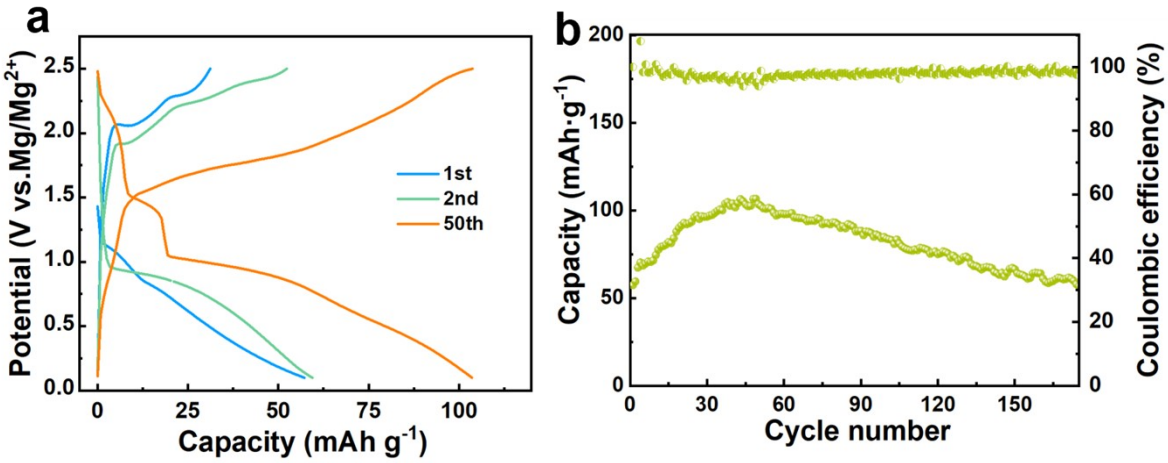

Fig. S12. (a) Charge/discharge profiles and (b) cycling performance of Cu_2S-AHP electrode at 100 mA g^{-1}.

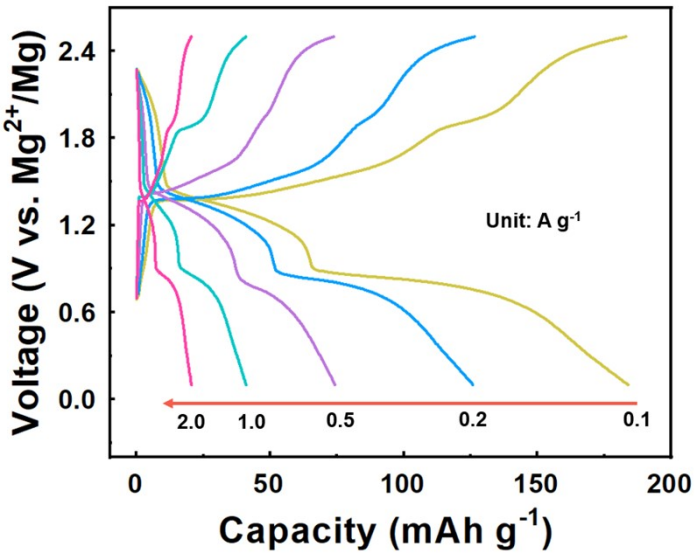

Fig. S13. Charge/discharge profiles of CuSe electrode at different current densities.

Table S1 Comparison of the present results with previous reports.

Materials	Electrolyte	Voltage range(V)	Current density (mA g^{-1})	Capacity (mAh g^{-1})	Ref
CuSe-AHP	$Mg(TFSI)_2$-$MgCl_2$/DME	0.1~2.5	100	227.6	This work
			1000	87.5	
CuSe nanoparticles	0.25 M $Mg(AlCl_2EtBu)_2$/THF	0.2~2.0	100	65	1
$CoSe_2$	0.5 M Mg-HMDS/G4	0.1~2.5	100	150	2
Sb_2Se_3	0.5 M Mg-HMDS/G4	0.1~2.2	1000	60	3
$MoSe_2$/C	0.4 M $(PhMgCl)_2$-0.2 M $AlCl_3$-0.5 M LiCl/THF	0.1~1.8	200	89	4
C−$Cu_{2-x}Se$	0.2 M Mg-HMDS/DME	0.3~2.2	100	138	5
			1000	48	5
$NiCo_2Se_4$	0.3 M Mg-HMDS$AlCl_3$/G4	0.01~2.8	2000	40	6
Ag_2Se@C	0.2 M APC/THF	0.3~1.9	100	182	7
$Ni_{0.85}Se$	0.4 M APC/THF+0.4 M LiCl	0.01~2.5	500	92	8
H-$CoSe_2$	0.2 M Mg-HMDS/G4/$MgCl_2$	0.01~2.6	50	110	9
			500	74	9
MoS_2	APC	0.01~2.4	100	60	10
			200	50	10
MoS_3	0.2 M Mg-HMDS/DME	0.3~2.6	100	175	11
			1000	75	
Cu_9S_5	0.2 M Mg-HMDS/DME	0.1~2.2	100	180	12
			1000	88	
V_2O_5	0.25 M $Mg(AlCl_2EtBu)_2$/THF	0.4~2.0	200	60	13

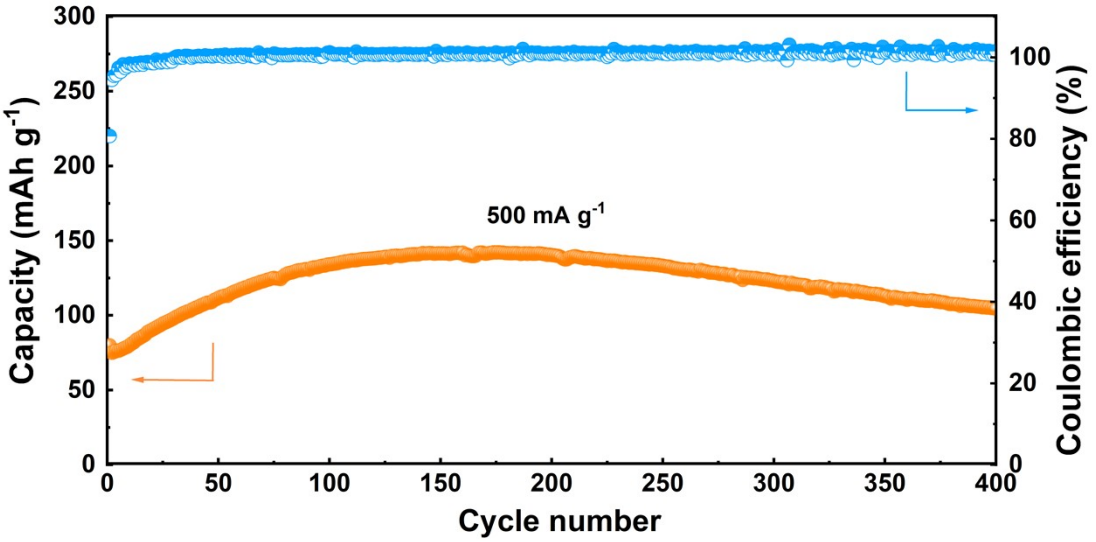

Fig.S14. Cycling performance of CuSe-AHP electrode at 500 mA g^{-1}.

Table S2 EIS simulation results of CuSe-AHP and CuSe electrodes after the first and 50th cycles in RMBs using the equivalent circuit as below.

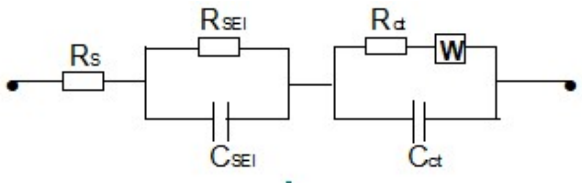

Cycle	CuSe-AHP			CuSe		
	R_s (Ω)	R_{SEI} (Ω)	R_{ct} (Ω)	R_s (Ω)	R_{SEI} (Ω)	R_{ct} (Ω)
1st	19.4	11.4	196.8	21.2	14.3	256.5
50th	22.9	14.9	172.3	33.2	26.5	284.2

R_s, R_{SEI} and R_{ct} are the resistances of solution, solid electrolyte interface (SEI) film and charge transfer, respectively. W represents Warburg impedance

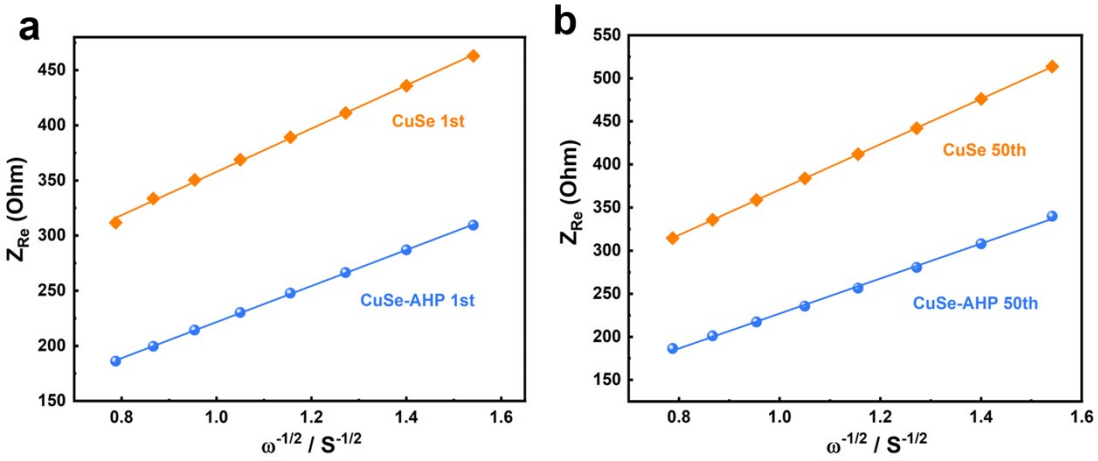

Fig. S15. Linear fitting of Z_{Re} with negative square root of angular frequency ($\omega^{-1/2}$) in the low frequency diffusion region for CuSe-AHP and CuSe electrodes after (a) the 1st cycle and (b) 50th cycle.

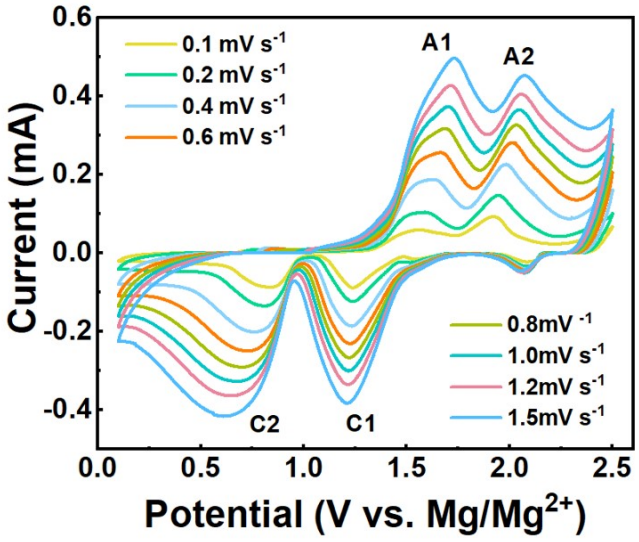

Fig. S16. CV profiles of CuSe electrode at different scan rates.

Table S3. The results of Mg^{2+} diffusion coefficient of CuSe-AHP and CuSe electrodes calculated from CV.

Peak	CuSe-AHP		CuSe	
	$i_p/v^{1/2}$	D ($\times 10^{-11}$ cm^2 s^{-1})	$i_p/v^{1/2}$	D ($\times 10^{-11}$ cm^2 s^{-1})
C1	0.0403	2.6862	0.0304	2.0246
C2	0.0490	3.2232	0.0306	2.0835
A1	0.0526	3.5024	0.0343	2.3528
A2	0.0477	3.1708	0.0352	2.4047

The Mg^{2+} diffusion coefficient is calculated by the following equation:[14]

$$i_p = 2.69\times10^5 n^{3/2} A D^{1/2} v^{1/2} C_0 \qquad \text{(S1)}$$

where i_p is the peak current (A), n is the number of electrons per molecule during the reaction, A is the contact area between the electrode and electrolyte, D is the diffusion coefficient of Mg^{2+} (cm^2 s^{-1}), C_0 is the concentration of Mg^{2+} in the electrode material (mol m^{-3}), and v is the scan rate (V s^{-1}).

Table S4. The results of Mg^{2+} diffusion coefficient of CuSe-AHP and CuSe electrodes calculated from GITT.

	$D_{Mg^{2+}}$ (10^{-11} cm^2 s^{-1})	
	CuSe-AHP	**CuSe**
Peak C_1	2.4997 (1.21V)	1.5883 (1.20V)
Peak C_2	3.2107 (0.80V)	2.6254 (0.81V))
Peak A_1	3.8875 (1.49V)	2.4225 (1.50V)
Peak A_2	2.8709 (1.82V)	1.9529 (1.82V)

The Mg-ion diffusion coefficients ($D_{Mg^{2+}}$) of CuSe-AHP and CuSe electrodes can be calculated based on the following equation.[15]

$$D_{Mg^{2+}} = \frac{4}{\pi\tau}\left(\frac{m_B V_m}{M_B A}\right)^2 \left(\frac{\Delta E_s}{\Delta E_\tau}\right)^2 \quad \text{(S2)}$$

where V_m, M_B and m_B are the molar volume, the molar mass and the weight of the compound, respectively, A is the active surface area of the electrode, τ is the charging or discharging time within one procedure, ΔE_τ and ΔE_s represent the total voltage change during the current pulse and the steady-state voltage change at the plateau potential, respectively.

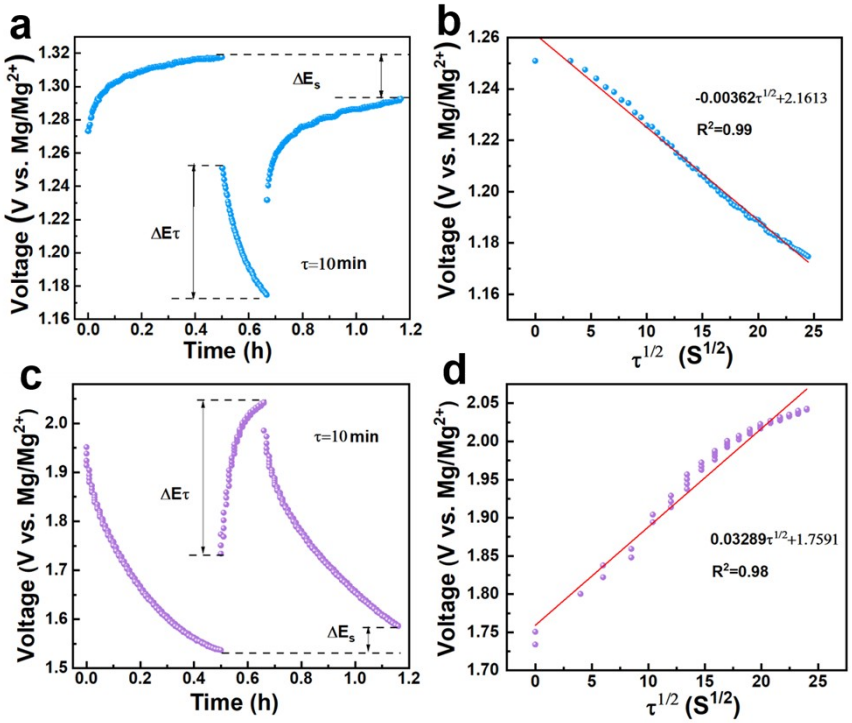

Fig. S17. A single GITT titration and the corresponding linear behavior of E vs. $\tau^{1/2}$ relationship of CuSe-AHP electrode at (a, b) discharged from 0.91V to 0.82V and (c, d) charged from 1.96V to 2.25V.

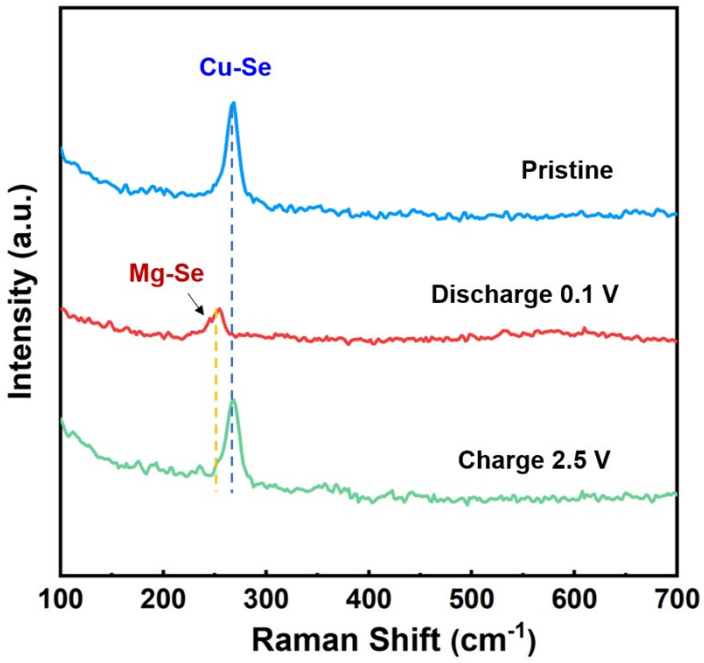

Fig. S18. Raman spectra of CuSe-AHP electrode at different charge/discharge states.

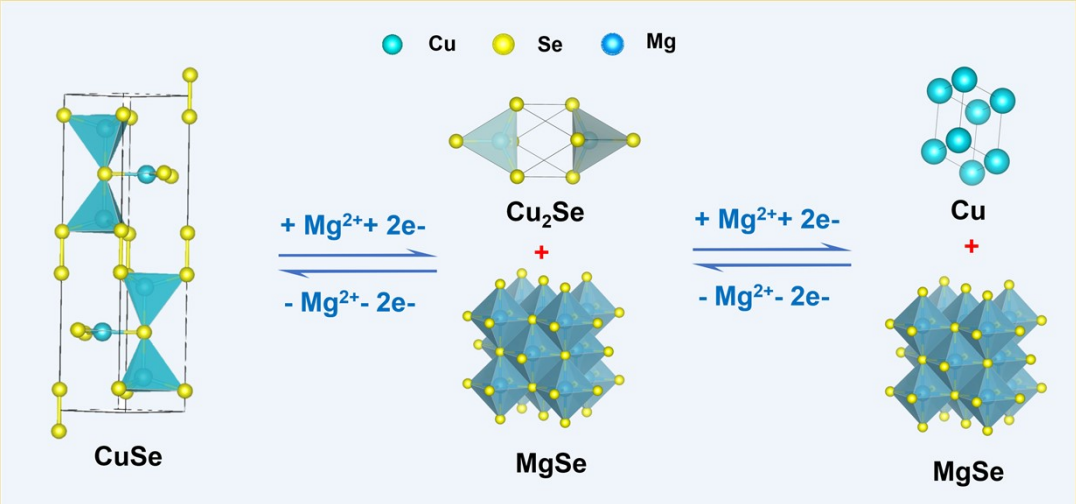

Fig. S19. Schematic illustration for magnesium-storage mechanism of CuSe-AHP electrode.

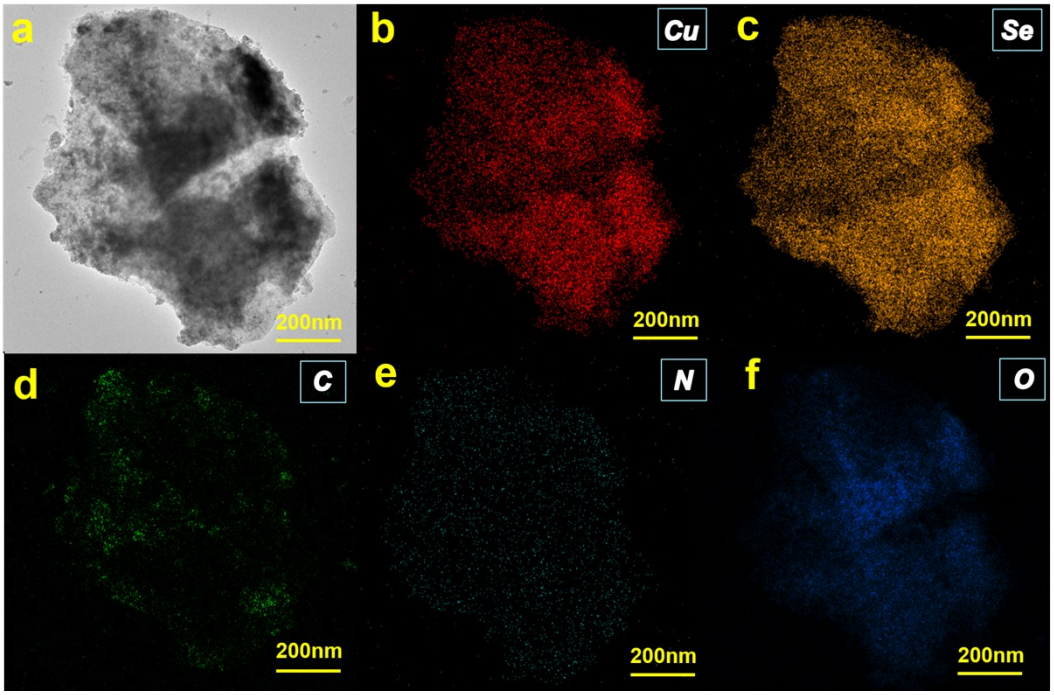

Fig. S20. (a) TEM image and (b-f) corresponding elemental (Cu, Se, C, N, O) mapping images of CuSe electrode after 50 cycles.

References

1 S. Yang, F. Ji, Z. Wang, Y. Zhu, K. Hu, Y. Ouyang, R. Wang, X. Ma, C. Cao, *Electrochim Acta* 2019, *324*, 134864.

2 D. Chen, F. Du, S.-a. Cao, T. Li, F. Xu, *Chem. Eng. J.* 2022, *428*, 129545.

3 D. Chen, Y. Zhang, J. Shen, X. Li, Z. Chen, S. Cao, T. Li, F. Xu, *Dalton Trans.* 2019, *48*, 17516-17523.

4 J.-J. Fan, S.-Y. Shen, Y. Chen, L.-N. Wu, J. Peng, X.-X. Peng, C.-G. Shi, L. Huang, W.-F. Lin, S.-G. Sun, *Electrochem. Commun.* 2018, *90*, 16-20.

5 D. Chen, Y. Zhang, X. Li, J. Shen, Z. Chen, S.-A. Cao, T. Li, F. Xu, *Chem. Eng. J.* 2020, *384*, 123235.

6 Y. Zhang, T. Li, S.-A. Cao, W. Luo, F. Xu, *ACS Sustainable Chem. Eng.* 2020, *8*, 2964-2972.

7 J. H. Ha, B. Lee, J. H. Kim, B. W. Cho, S.-O. Kim, S. H. Oh, *Energy Stor. Mater.* 2020, *27*, 459-465.

8 D. Chen, J. Shen, X. Li, S.-A. Cao, T. Li, W. Luo, F. Xu, *J. Energy Chem.* 2020, *48*, 226-232.

9 D. Chen, Y. Zhang, X. Li, J. Shen, Z. Chen, S.-A. Cao, T. Li, F. Xu, *Nanoscale.* 2019, *11*, 23173-23181.

10 F. Zhu, H. Zhang, Z. Lu, D. Kang, L. Han, *J. Energy Stor.* 2021, *42*, 103046.

11 Y. Zhang, D. Chen, X. Li, J. Shen, Z. Chen, S. A. Cao, T. Li, F, Xu, *Nanoscale*. 2019, *11*, 16043.

12 M. Wu, Y. Zhang, H. Wu, A. Qin, X. Li, J. Shen, Z. Chen, S. A. Cao, T. Li, F. Xu, *Energy Technol.* 2019, *7*, 1800777.

13 Y. Xiao, M. Pan, J. Zou, R. Guo, X. Zeng, W, Ding, *Ionics* 2019, *25*, 5889-5997.

14 Z. Wei, D. Wang, M. Li, Y. Gao, C. Wang, G. Chen, F. Du, *Adv. Energy Mater.* 2018, *8*, 1801102.

15 C. Pei, F. Xiong, J. Sheng, Y. Yin, S. Tan, D. Wang, C. Han, Q. An, L. Mai, *ACS Appl. Mater. Interfaces* 2017, *9*, 17060-17066.